Mapping the Transmural Scar and Activation for Patients with Ventricular Arrhythmia

Linwei Wang[1], Fady Dawoud[2], Ken CL Wong[1], Heye Zhang[3], Huafeng Liu[4], John Sapp[5],Milan Horáček[5], Pengcheng Shi[1]

[1]Computational Biomedicine Laboratory, Rochester Institute of Technology, Rochester, NY, USA
[2] Johns Hopkins University Medical School, Baltimore, MD, USA
[3] Shenzhen Institutes of Advanced Technology, Shenzhen, China
[4]State Key Laboratory of Modern Optical Instrumentation,Zhejiang University, Hangzhou, China
[5] Dalhousie University, Halifax, Nova Scotia, Canada

Abstract

Myocardial scar is the most common substrate for malignant arrhythmia and cardiac arrest. Radiofrequency ablation, as one of the emerging mainstream therapies, currently relies on electrophysiologic (EP) map acquired on endocardial and occasionally epicardial surfaces. As myocardial scar is often complex with shapes varying with the depth of the myocardium, endocardial and epicardial maps may differ substantially, and may fail to identify mid-wall fibrosis that exist in $\sim 30\%$ of patients with nonischemic cardiomyopathy. Alternative image-based delineation of anatomical scar is noninvasive and transmural, but it does not reflect the possibly EP functional anomaly. In this paper, we present a validation study of a previously developed method that combines body-surface electrocardiographic data and image-derived anatomic data to compute EP and scar details along the depth of the myocardium. Experiments were performed on 4 patients referred for ablation associated with myocardial infarction, with gold standards *of substrate voltage maps and activation maps acquired by CARTO electroanatomic mapping system. This study exhibits the ability of the presented method in accurately quantifying the scar substrate and capturing abnormal EP patterns, not only on the heart surfaces but along the transmural dimension.*

1. Introduction

Myocardial scar is the most common substrate for ventricular arrhythmia such as tachycardia (VT), which could result in hemodynamic collapse with syncope or sudden death if sustained. The current state of the art for VT ablation relies on the voltage or activation sequence maps acquired during electrophysiologic (EP) mapping, performed by moving the mapping catheter from site to site on endocardial and occasionally epicardial surfaces. Besides being time consuming and technical challenging, this invasive, point-to-point EP mapping is confined to heart surfaces with limited measurement sites. As myocardial scar is often complex with shapes varying with the depth of the myocardium, endocardial and epicardial maps may differ substantially, and may fail to identify mid-wall fibrosis that exist in $\sim 30\%$ of patients with nonischemic cardiomyopathy [1].

High-resolution delay contrast enhanced imaging [2] is a relatively new technique able to characterize myocardial necrosis in the transmural dimension. Enhancing structural scars, these imaging approaches do not offer the associated subject-specific EP details or therefore the possible EP functional anomalies. It remains also an open question as to the correlation between the enhanced anatomical scar and the electrically-defined scar substrate.

Computational methods have been developed to calculate subject-specific EP activity of the heart using noninvasive body-surface electrocardiographic data and image-derived anatomic data, from the spatiotemporal features of which electroanatomic substrates can then be delineated. The mainstream research approaches obtain solutions on heart surfaces, in terms of pericardial electrocardiograms [3] or activation/recovery time on the entire epi- and endocardial surfaces [4]. Despite the advantage of noninvasive, beat-to-beat mapping, surface solutions still lack information on the transmural dimension. Combining computational modeling into probabilistic estimation, we developed a novel method to use body-surface electrocardiographic data to infer transmural subject-specific EP dynamics not only on heart surfaces but deep into the myocardium [5]. Real-data validations were performed on 4 patients with previous myocardial infarction (MI) with infarct documented by DE-MRI imaging [6].

In this paper, we present an experimental validation

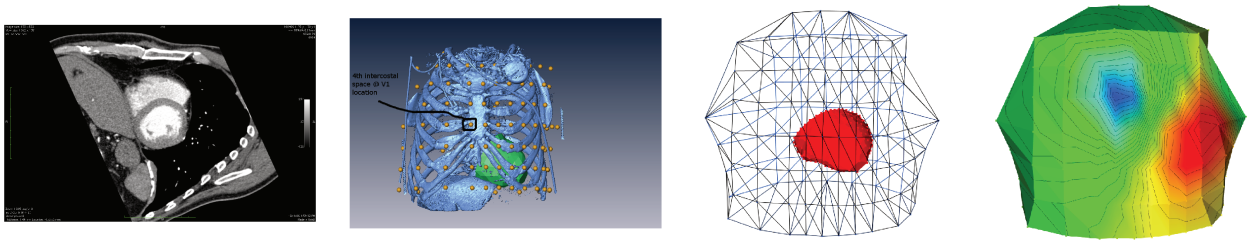

(a) (b) (c) (d)

Figure 1. (a) Short-axis view of the heart provided by the volume CT scan. (b) Electrodes of *Dalhousie* 120-lead mapping systems as documented by the CT image on the body surface. (c) Image-derived computational model of personalized geometry. (d) Snapshot of a sinus-rhythm body-surface potential map (color-encoded, blue and red represent the minimum and maximum) at 280 ms after the onset of ventricular activation.

study on 4 patients who were referred to VT ablation associated with MI and underwent multi-point catheter mapping performed with CARTO electroanatomic mapping system during sinus-rhythm and pacing with implantable cardioverter defibrillator (ICD). CT and body-surface electrocardiographic data of each patient were acquired for transmural EP and scar imaging. Compared to validation study using DE-MRI images, CARTO maps allow to evaluate not only the accuracy of 17-segment based scar sizing, but also the accuracy of EP activation pattern.

2. Methods

Experimental Materials and Data: All the 4 patients were referred for ablation of VT associated with MI, having a history of VT resistant to antiarrhythmic drugs, ICD devices and recurrent device therapies.

Input data: The presented method gathered input patient-specific information from two sources of noninvasive data: body-surface electrocardiographic recordings and whole-body tomographic scans. Body-surface potential (BSP) maps were recorded by a 120-lead electrode-array according to the *Dalhousie* standard protocol [7] at $2k$Hz. Axial 0.8mm-3mm CT scans were acquired in supine position and used to construct subject-specific geometry model as described previously [5]. Briefly, 3D myocardium is presented by unconnected (meshfree) points and anisotropic conduction is included in the 3D fiber structure mapped from the *Auckland* mathematical model of ventricular fibrous structure [8]. Personalized torso model, assumed to be homogenous, is obtained by deforming the standard *Dalhousie* torso model [7] to electrodes or landmarks identified in CT images. Fig. 1 gives an example of the short-axis cardiac CT slices (a) used in ventricular segmentation, the body-surface electrodes documented on the subject (b), the image-derived anatomic model (c), and a snapshot of the recorded BSP maps (d).

Validation data: Multi-point catheter mapping were performed by the CARTO electroanatomic mapping system using Navistar^{TM} Thermocool^{TM} 3.5-mm irrigated tip

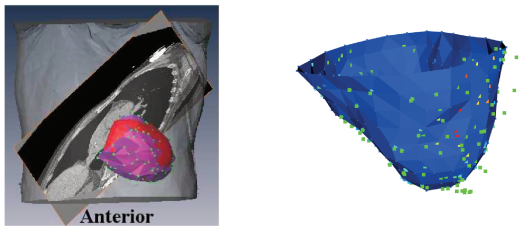

(a) (b)

Figure 2. (a) Anterior view of segmented torso shows oblique CT slice cutting through the atrio-ventricular ring to facilitate segmentation of the ventricles; CARTO surface (purple, constructed from green sampling sites) is manually aligned to the image-derived ventricles (red). (b) After alignment, CARTO points (green) were perpendicularly projected to the CT-derived surface (blue); color of the projected points encodes the projection distance.

with 3-pole 2-5-2-mm electrode spacing. Epicardial and/or endocardial bipolar voltage maps and activation maps were recorded both by the CARTO system and GE Cardiolab system, during sinus-rhythm for 2 patients and ICD-pacing for the other 2 patients. Spatial registration was performed manually between the CARTO surface (purple) and the CT data of each patient (Fig. 2 (a)). After alignment, CARTO mapping points (green) were perpendicularly projected to the surfaces of the CT-derived ventricle model of each subject. Fig. 2 (b) illustrates the locations of 146 CARTO points after perpendicular projection to the image-derived epicardial surface of one patient, with projection distance $= 4.71 \pm 3.93$mm (min: 0.06mm; max: 15.75mm).

Transmural EP and Scar Imaging: Without proper constraints, there is no unique solution of transmural EP dynamics for a given BSP distribution [9]. In our approach, a simple two-variable, phenomenological model of transmembrane potential (TMP) dynamics (*Aliev-Panfilov* model) [10] is used as the physiological constraints and estimation of subject-specific transmural TMP dynamics is formulated into *maximum a posteriori* probabilistic es-

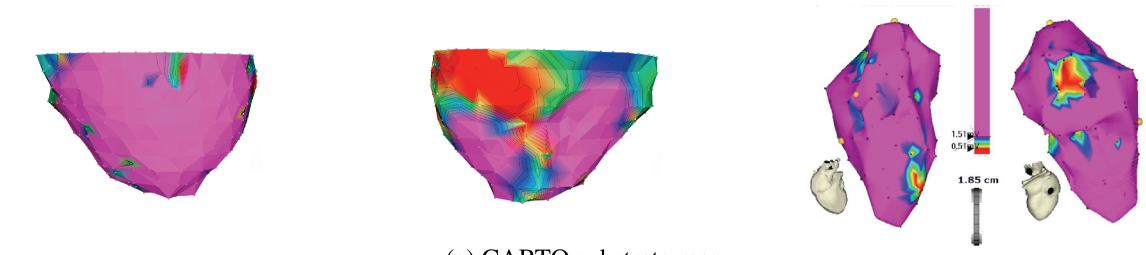

(a) CARTO substrate map

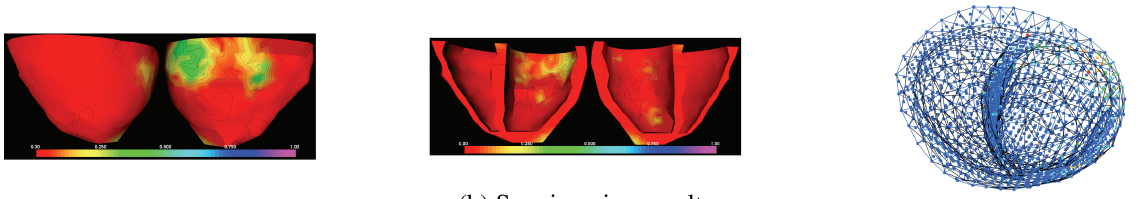

(b) Scar imaging results

Figure 3. (a) Left to right: epicardial anterior, epicardial inferior, endocardial anterior, endocardial inferior. (b). Left to right: epicardial, endocardial, transmural. Color bar encodes the feature values for infarct detection.

Table 1. Infarct quantification compared with CARTO reference. Estimated infarct segments are in descending order of injury percentage. Color blue highlights true-positives.

	CARTO		Results	
	Extent	Segments	Extent	Segments
AW	20%	1,4,5,6	19%	4,5,6,1
DC	23%	1,4,5,10,11	18%	5,4,10,11,6
EC	18%	6,11,12,16	11%	6,11,5, 16

timation to take into account the uncertainty that exist in the generic models and the input data. TMP estimation was carried out based on the unscented Kalman filter [11] to accommodate the nonlinearity and high dimensionality of this problem. Model and data errors were assumed to be zero-mean Gaussian noises with predefined covariance matrices. After computing the personalized transmural TMP dynamics, activation time (AT) and action potential duration (APD) were extracted and their deviances from normal conditions were equally weighted to generate a new feature that characterizes electrical conduction abnormality. K-means clustering was applied on this feature to discriminate between healthy and electrophysiologically-altered tissues. For more details refer to [5, 6].

3. Results

Scar Delineation: Quantitative accuracy of scar extent and location were positively validated on the image-derived epicardium by CARTO voltage maps of 3 patients (Table 1). As an example, Fig 3 (a) shows the reference bipolar voltage maps recorded at multiple CARTO sampling sites on the epicardium and endocardium of DC, where regions with amplitudes $< 0.5mV$ (red) were considered scar tissue, and regions with amplitudes of 0.5-1.5mV (green-blue) were border zone between dense car and normal tissue. Fig 3 (b) shows our results of 3D scar delineation on the same geometry, where the infarct location and extent on the epicardium were faithfully reconstructed on the epicardium, both qualitatively and quantitatively. The endocardial and transmural view of our results illustrates the scar details along the transmural dimension that was not available in CARTO data, and the endocardial delineation of basal-inferior and apical-lateral scar was confirmed by the endocardial CARTO voltage maps.

Activation Imaging: In the following we investigated this method in imaging the activation pattern paced by ICD devices. As shown in the epicardial CARTO activation map in Fig 4 (a), patient EC was paced by the ICD device located at RV anterior-apex: the activation spreads sequentially from RV through free wall to LV, and reaches basal region of posterior LV in the last with a total activation time (TAT) 266ms; patient RX was paced at RV inferior-apex: the activation then spreads sequentially and reaches basal region of anterior LV in the last with a TAT 255ms.

Fig 4 (b.1) illustrates the sinus-rhythm activation sequence simulated from the *a priori*, normal TMP model of EC, where LV and RV were activated simultaneously and differed drastically from the specific ICD-pacing condition of EC; the latest activation reaches at RV basal freewall with a much shorter TAT 65ms. Fig 4 (b.2) shows the activation time computed under the constraints of (b.1), which captured the early activation at RV anterior-apex caused by the pacing device, as well as the sequential activation through RV free wall to posterior-lateral LV, with a TAT $= 220ms$. Similarly, Fig 4 (c) shows the simulated normal, sinus-rhythm activation versus computed activation of RX, where again the constraints of simultaneous ventricular activation (TAT $= 70ms$) with latest basal RV activation was corrected to reflect the early activation at RV inferior-apex, as well as the sequential activation through

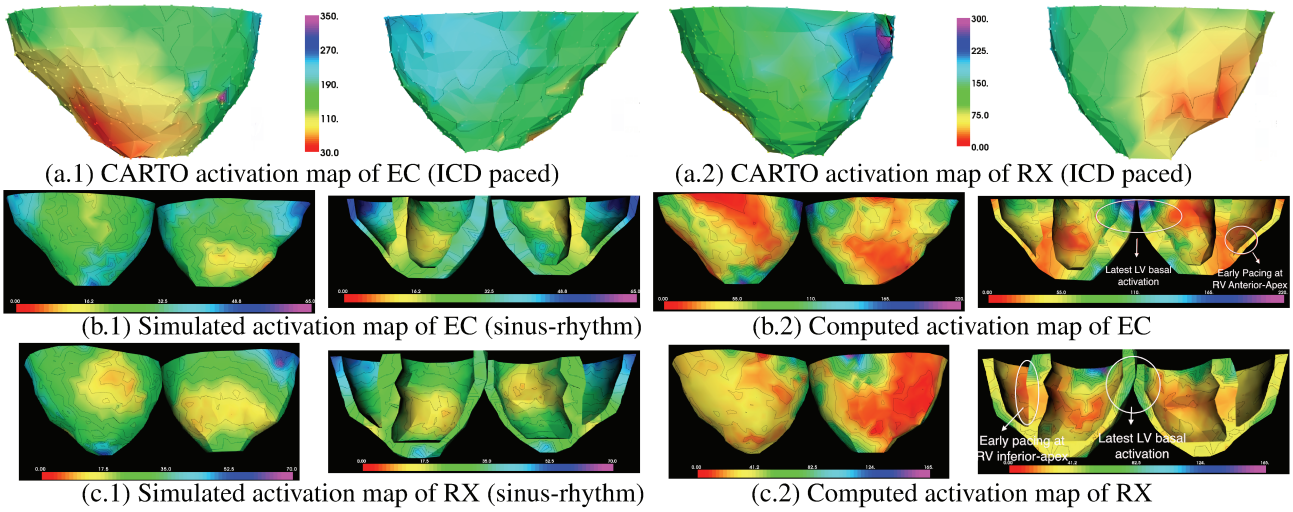

(a.1) CARTO activation map of EC (ICD paced) (a.2) CARTO activation map of RX (ICD paced)

(b.1) Simulated activation map of EC (sinus-rhythm) (b.2) Computed activation map of EC

(c.1) Simulated activation map of RX (sinus-rhythm) (c.2) Computed activation map of RX

Figure 4. Comparison of CARTO activation maps (a) with simulated activation maps assuming sinus-rhythm on healthy hearts (b.1 and c.1), and activation maps computed under the sinus-rhythm constraints (b.2 and c.2).

RV free wall to anterior-lateral LV with a TAT $= 165ms$.

Discussions: With constraints assuming sinus-rhythm activation on a healthy heart, the presented method showed high accuracy in quantifying the extent and location of infarct substrate, and exhibited its ability to qualitatively capture the early activation caused by pacing, the abnormal activation pattern as well as the elongated total activation time. However, because the current algorithm iteratively uses the arriving BSP data to correct the constraints and converges in time, it is difficult to precisely correct the erroneous initial conditions of regular sinus-rhythm excitation as shown in Fig 4. This does not impact the accuracy of scar imaging that considered the differences between the simulated constraints and the computed results. For a more precise imaging of patient-specific EP activity, nevertheless, we plan to upgrade the filtering algorithm to smoothing algorithm so the erroneous constraints are not corrected only by the BSP measurement available until the current time instant but by the complete BSP sequence.

This validation study involves many uncertain errors introduced in the data acquisition and processing procedure, include the alignment of CARTO data and image data, and the projection of CARTO points to image-derived model. Furthermore, the validation using data from point-by-point mapping requires care in data recording and processing because of the beat-beat variability and occasional preventricular complexes (PVC's).

References

[1] Nazarian S, Bluemke DA, Lardo AC, et al. Magnetic resonance assessment of the substrate for inducible ventricular tachycardia in nonischemic cardiomyopathy. Circulation 2005;112:2821–2825.

[2] Ashikaga H, et al. Magnetic resonance-based anatomical analysis of scar-related ventricular tachycardia. implications for catheter ablation. Circ 2007;101:939–947.

[3] Rudy Y, Messinger-Rapport B. The inverse problem of electrocardiography: solutions in terms of epicardial potentials. CRC Critical Reviews on Biomedical Engineering 1988;16:215–268.

[4] Dam PMV, Oostendorp TF, Linnenbank AC, van Oosterom A. Non-invasive imaging of cardiac activation and recovery. Annals of Biomedical Engineering 2009;37(9):1739–1756.

[5] Wang L, Zhang H, Wong K, Liu H, Shi P. Physiological-model-constrained noninvasive reconstruction of volumetric myocardial transmembrane potentials. IEEE Trans Biomed Eng 2010;5(2):296–315.

[6] Wang L, Zhang H, Wong K, Liu H, Shi P. Noninvasive computational imaging of cardiac electrophysiology for 3-d infarct. IEEE Trans Biomed Eng 2011;58(4):1033–1043.

[7] Title LM, Iles SE, Gardner MJ, Penney CJ, Clements JC, Horacek BM. Quantitative assessment of myocardial ischemia by electrocardiographic and scintigraphic imaging. J Electrocardiol 2003;36(Suppl):17–26.

[8] Nash M. Mechanics and Material Properties of the Heart using an Anatomically Accurate Mathematical Model. Ph.D. thesis, Univ. of Auckland, New Zealand, May 1998. URL `http://www.esc.auckland.ac.nz/Nash/thesis/`.

[9] Plonsey R. Bioelectric phenonmena. New York: McGraw Hill, 1969.

[10] Aliev RR, Panfilov AV. A simple two-variable model of cardiac excitation. Chaos Solitions Fractals 1996;7(3):293–301.

[11] Julier S. The scaled unscented transform. Int J Numer Meth Eng 2000;47:1445–1462.

Address for correspondence:

Linwei Wang
Rm 74-1075, 102 Lomb Memorial Dr., Rochester, NY 14534.
linwei.wang@rit.edu